Wettability switching techniques on superhydrophobic surfaces

N. Verplanck, Yannick Coffinier, V. Thomy, Rabah Boukherroub

Nanoscale Res Lett (2007) 2:577–596
DOI 10.1007/s11671-007-9102-4

NANO REVIEW

Wettability Switching Techniques on Superhydrophobic Surfaces

Nicolas Verplanck · Yannick Coffinier · Vincent Thomy · Rabah Boukherroub

Received: 27 June 2007 / Accepted: 22 October 2007 / Published online: 13 November 2007

Abstract The wetting properties of superhydrophobic surfaces have generated worldwide research interest. A water drop on these surfaces forms a nearly perfect spherical pearl. Superhydrophobic materials hold considerable promise for potential applications ranging from self cleaning surfaces, completely water impermeable textiles to low cost energy displacement of liquids in lab-on-chip devices. However, the dynamic modification of the liquid droplets behavior and in particular of their wetting properties on these surfaces is still a challenging issue. In this review, after a brief overview on superhydrophobic states definition, the techniques leading to the modification of wettability behavior on superhydrophobic surfaces under specific conditions: optical, magnetic, mechanical, chemical, thermal are discussed. Finally, a focus on electrowetting is made from historical phenomenon pointed out some decades ago on classical planar hydrophobic surfaces to recent breakthrough obtained on superhydrophobic surfaces.

Keywords Microfluidic · Superhydrophobic surfaces · Wettability switching · Electrowetting

N. Verplanck · Y. Coffinier · V. Thomy (✉) · R. Boukherroub
Institut d'Electronique, de Microélectronique et de Nanotechnologie (IEMN), UMR 8520, Cité Scientifique, Avenue Poincaré, B.P. 60069, 59652 Villeneuve d'Ascq, France
e-mail: vincent.thomy@iemn.univ-lille1.fr

Y. Coffinier · R. Boukherroub
Institut de Recherche Interdisciplinaire (IRI), FRE 2963, Cité Scientifique, Avenue Poincaré, B.P. 60069, 59652 Villeneuve d'Ascq, France

Introduction

Biological surfaces, like lotus leaves, exhibit the amazing property for not being wetted by water leading to a self cleaning effect. The lotus leaves capability to remain clean from dirt and particles is attributed to the superhydrophobic nature of the leaves surface. The latter is composed of micro and nano structures covered with a hydrophobic wax, creating a carpet fakir, where water droplets attained a quasi spherical shape. In order to mimic these properties, artificial superhydrophobic surfaces have been prepared by several means, including the generation of rough surfaces coated with low surface energy molecules [1–6], roughening the surface of hydrophobic materials [7–9], and creating well-ordered structures using micromachining and etching methods [10, 11].

However, the modification of the liquid droplets behavior and in particular of their wetting properties on these surfaces is still a challenging issue. Functional surfaces with controlled wetting properties, which can respond to external stimuli, have attracted huge interest of the scientific community due to their wide range of potential applications, including microfluidic devices, controllable drug delivery and self cleaning surfaces.

In this review, after a brief overview on superhydrophobic states definition, we will discuss the techniques leading to the modification of wettability behavior on superhydrophobic surfaces under specific conditions: optical, magnetic, mechanical, chemical, thermal… Finally, a focus on electrowetting will be made from historical phenomenon pointed out some decades ago on classical planar hydrophobic surfaces to recent breakthrough obtained on superhydrophobic surfaces.

Surface Wetting

Introduction

The wetting property of a surface is defined according to the angle θ, which forms a liquid droplet on the three phase contact line (interface of three media—Fig. 1a). A surface is regarded as wetting when the contact angle, which forms a drop with this one, is lower than 90° (Fig. 1a). In the opposite case (the contact angle is higher than 90°), the surface is nonwetting (Fig. 1b). For water, the terms "hydrophilic" and "hydrophobic" are commonly used for wetting and nonwetting surfaces, respectively.

The contact angle of a liquid on a surface according to the surface tension is given by the relation of Young (1). The surface tension, noted γ, is the tension which exists at the interface of two systems (solid/liquid, liquid/liquid, solid/gas). It is expressed in energy per unit of area (mJ m^{-2}), but can also be regarded as a force per unit of length (mN m^{-1}). From this definition, it is possible to identify three forces acting on the three phase contact line: γ_{LG} (liquid surface stress/gas), γ_{LS} (liquid/solid surface stress) and γ_{SG} (solid surface stress/gas). The three forces are represented in Fig. 2.

At the equilibrium state:

$$\vec{\gamma}_{LS} + \vec{\gamma} + \vec{\gamma}_{SG} = 0$$

By projection on the solid, the relation of Young [12] is obtained:

$$\gamma_{LS} = \gamma_{SG} - \gamma \cos\theta_0 \quad (1)$$

It is also possible to establish the Eq. 1 by calculus of the surface energy variation related to a displacement dx of the three phase contact line:

$$dE = (\gamma_{LS} - \gamma_{SG})dx + \gamma dx \cos\theta$$

At the equilibrium state, using energy minimization ($dE = 0$), the Young relation (**1**) is found. This approach will be used thereafter to determine the relations of Wenzel and Cassie–Baxter on superhydrophobic surfaces.

Concretely, following the rule of Zisman [13, 14], wetting surfaces are surfaces of high energy (~500–5,000 mN m^{-1}), where the chemical binding energies are about an eV (ionic, covalent, metal connections). The wetting materials are typically oxides (glass), metal oxides,… On the other hand, nonwetting surfaces are characterized by low surface energy (~10–50 mN m^{-1}). For these materials, the binding energies are about kT (ex: crystalline substrates and polymers) [15].

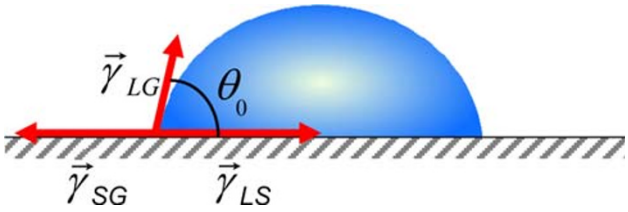

Fig. 2 Surface forces acting on the three phase contact line of a liquid droplet deposited on a substrate

Hysteresis

The hysteresis of a surface is related to its imperfections. Indeed, the formula of Young considers that there is only one contact angle, the static contact angle, noted θ_0. However, this configuration exists only for perfect surfaces. Generally, surfaces present imperfections related to physical defects like roughness or to chemical variations. The static contact angle thus lies between two values called advanced angle, noted θ_A, and receding angle, noted θ_R. The difference between these two angles ($\theta_A - \theta_R$) is called hysteresis. While this force is opposed to droplet motion, the smaller hysteresis is, the more it will be easy to move the liquid droplet. Concretely, these angles can be measured thanks to the shape of a droplet on a tilted surface (Fig. 3).

Wetting on Superhydrophobic Surfaces: Wenzel and Cassie–Baxter States

The lotus leaves are known for their water repellency and consequently to remain clean from any parasitic dust or debris. This phenomenon (also called rolling ball state) is very common in nature not only for the lotus, but also for

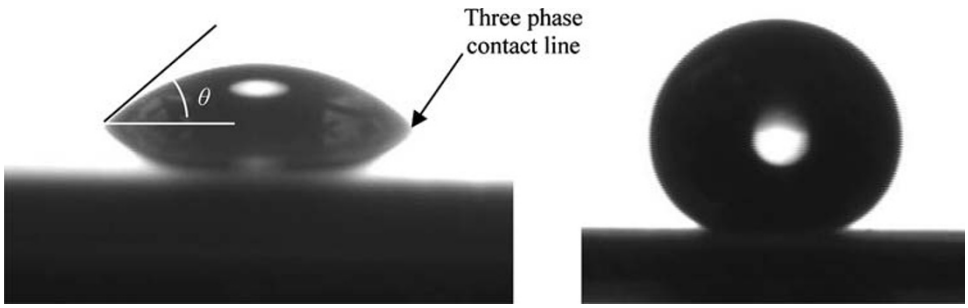

Fig. 1 Droplet of water deposited on two surfaces of different energies: (**a**) wetting surface ($\theta < 90°$), (**b**) nonwetting surface ($\theta > 90°$)

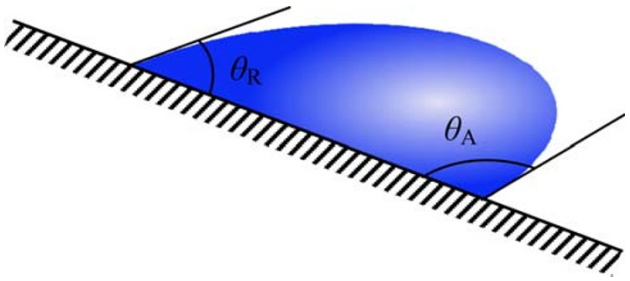

Fig. 3 Advanced θ_A and receding θ_R angles of a liquid droplet on a tilted surface

nearly 200 other species: vegetable and animal like species. For example, the wings of a butterfly are covered with shapes whose size and geometrical form lead to a superhydrophobic state and are at the origin of their color (Fig. 4).

The common point between all these surfaces is their roughness. Indeed, the surfaces are composed of nanometric structures limiting the impregnation of the liquid and pushing back the drop. Most of the time, the surfaces are made of a second scale of roughness, consisting of micrometric size. In order to minimize its energy, a liquid droplet forms a liquid pearl on the microstructured surface. The superhydrophobicity term is thus used when the apparent contact angle of a water droplet on a surface reaches values higher than 150°.

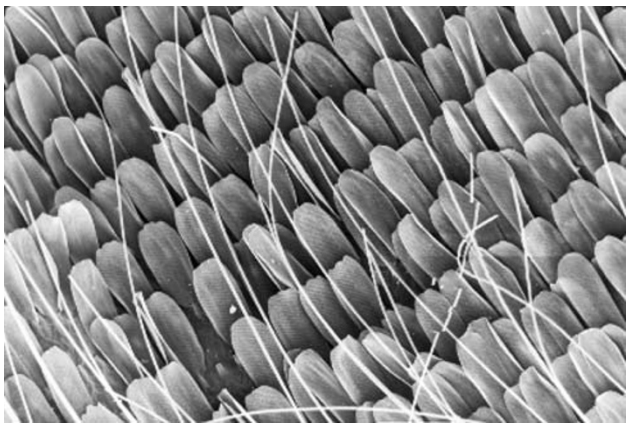

Fig. 4 SEM image of a butterfly wings [16]. Reprinted with permission. Copyright of The University of Bath (UK)

Previously, the studied substrates were regarded as smooth surfaces, i.e. the roughness of the substrate was sufficiently low and thus does not influence the wetting properties of the surface. In this case, the relation of Young (**1**) gives the value of the contact angle θ on the surface (which we will henceforth call angle of Young). However, a surface can have a physical heterogeneity (roughness) or a chemical composition variation (materials with different surface energies). In this case, a drop deposited on the surface reacts in several ways. A new contact angle is then observed, called apparent contact angle and generally noted θ^*. It should be noticed that locally, the contact angle between the liquid droplet and the surface are always the angle of Young. Two models exist: the model of Wenzel [17, 18] and of Cassie–Baxter [19].

These two models were highlighted by the experiment of Johnson and Dettre [20]. Many research teams have tried to understand in more detail the superhydrophobicity phenomenon [21] and particularly the difficulty of the wetting transition from Wenzel to Cassie configuration [22]. A drop on a rough and hydrophobic surface can adopt two configurations: a Wenzel [23] (complete wetting) and a Cassie–Baxter configuration (partial wetting), as presented in Fig. 5a and b, respectively. In both cases, even if locally, the contact angle does not change (angle of Young), an increase in the apparent contact angle θ^* of the drop is observed.

For a superhydrophobic surface, the fundamental difference between the two models is the hysteresis value. The first experiment on this subject was conducted by Johnson and Dettre (1964) who measured the advancing and receding contact angles, according to the surface roughness [20]. For a low roughness, a strong hysteresis being able to reach 100° (Wenzel) is observed and attributed to an increase in the substrate surface in contact with the drop. Starting from a certain roughness (not quantified in their experiment), the hysteresis becomes quasi null resulting from the formation of air pockets under the drop. The receding angle approaches the advancing angle.

Other experiments also show that for a drop, in a Cassie–Baxter state, it is possible to obtain a contact angle quite higher than for a drop in Wenzel state (Fig. 6a) [24]. The drop on the left is in a Cassie–Baxter state whereas the drop on the right is in a Wenzel state. After partial evaporation of the drop (Fig. 6b), the observed angle (which is

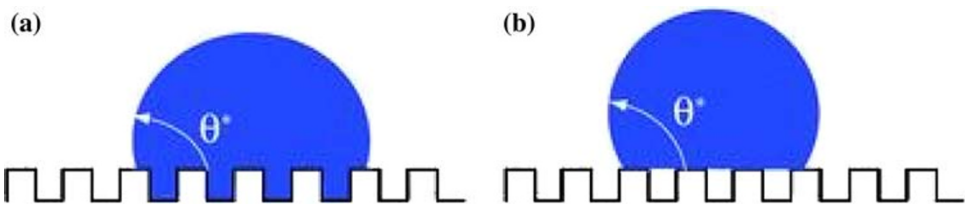

Fig. 5 Superhydrophobic surfaces: (**a**) Wenzel, (**b**) Cassie–Baxter model [24]. Reprinted with permission from [24]. Copyright 2007 Royal Society of Chemistry

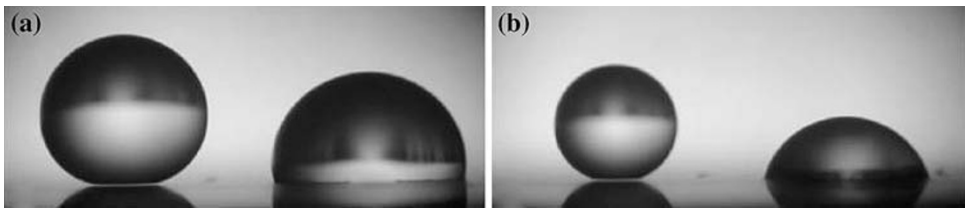

Fig. 6 Illustration of the difference between the Cassie–Baxter and Wenzel states: (**a**) after deposition of the liquid drops on the surface, (**b**) after evaporation [24]. Reprinted with permission from [24]. Copyright 2007 Royal Society of Chemistry

the receding angle) is similar to the advancing angle for the drop on the left whereas the drop on the right appears like trapped on a hydrophilic surface.

In the following two paragraphs, we will discuss in detail the two models. Then we will show that the reality is more complex, in particular in the presence of metastable states in the Cassie–Baxter model.

Wenzel (1936)

When a surface exhibits a low roughness, the drop follows the surface and is impaled on roughness (Fig. 5a). In this case, the solid surface/liquid and solid/gas energies are respectively $r\gamma_{SL}$ and $r\gamma_{SG}$, where the roughness r is defined as the relationship between real surface and apparent surface ($r > 1$ for a rough surface, and $r = 1$ for a perfectly smooth surface) [25]. A dx displacement of the three phase contact line thus involves a variation of energy:

$$dE = r(\gamma_{SL} - \gamma_{SV})dx + \gamma dx \cos\theta^* \quad (2)$$

At the equilibrium state ($dE = 0$), for a null roughness, i.e. for $r = 1$, we find the relation of Young. For a nonnull roughness, the relation of Wenzel [18] is obtained:

$$\cos\theta^* = r\cos\theta \quad (3)$$

The question is to know what are the conditions to be in this configuration? In this relation, the angle of Young θ cannot be modulated since on a planar surface the optimal contact angle value is around 120° for water. Moreover, this relation implies that it is possible to reach an apparent contact angle of 180° as soon as the product r cos θ reaches -1 (as shown in Fig. 7). However an apparent angle θ^* of 180° cannot be observed because the drop must preserve a surface of contact with the substrate. Thus the only parameter that can be modulated is the roughness. However, a strong roughness involves a configuration of Cassie–Baxter. Indeed, a liquid droplet rather minimizes its energy while remaining on a surface of a strong roughness than penetrating in the asperities. So the law of Wenzel is valid only for one certain scale of roughness and thus for apparent angles lower than 180°.

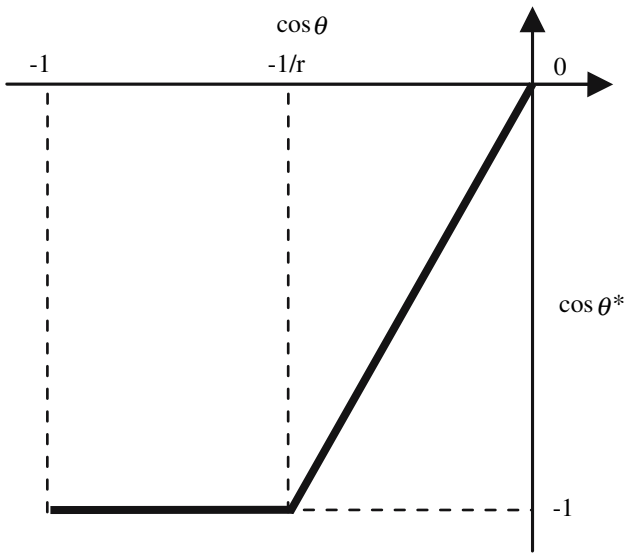

Fig. 7 Apparent contact angle according to the angle of Young (relation of Wenzel)

In this type of behavior, the liquid/solid interface and the hysteresis are strongly increased. The drop sticks to the surface and the Wenzel state contrasts with the superhydrophobicity idea i.e. the rolling ball effect.

Cassie–Baxter (1944)

Cassie and Baxter did not directly investigate the wetting behavior of liquid droplets on superhydrophobic surfaces. They were more particularly interested in planar surfaces with chemical heterogeneity (Fig. 8).

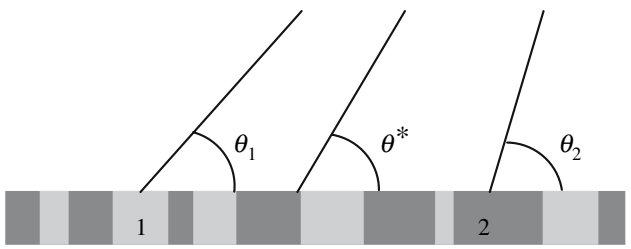

Fig. 8 Planar surface composed of two different and chemically heterogeneous materials

The examined surface consists of two materials; each one has its own surface energy, characteristic contact angle, and occupies a definite fraction of the surface. If material 1 is hydrophobic and material 2 is replaced by air, a drop in contact with each of the two phases (solid and air) forms respective contact angles θ_E and 180°, whereas the fractions of respective surfaces are Φ_s and $(1 - \Phi_s)$. Considering a displacement dx of the three phase contact line, the change of energy dE could be expressed by:

$$dE = \phi_S(\gamma_{SL} - \gamma_{SV})dx + (1 - \phi_S)\gamma dx + \gamma dx \cos\theta^* \quad (4)$$

By using the relation of Young, the minimum of E leads to the Cassie–Baxter relation:

$$\cos\theta^* = -1 + \phi_S(\cos\theta_E + 1) \quad (5)$$

It is to be noted that the apparent angle θ^* is included in the interval $[\theta_1, \theta_2]$. Figure 9 illustrates the behavior of the apparent Young angle according to the Cassie–Baxter relation (**5**).

To summarize, a low roughness involves a Wenzel configuration while a strong roughness a Cassie–Baxter one. De Gennes showed that for a sinusoidal surface and a Young angle of 120°, the roughness from which appear air pockets is 1.75 [15]. Moreover, Bico et al. demonstrated that the Cassie–Baxter mode is thermodynamically stable for a given value threshold cos θ_c [26]. The value of this angle can be determined when the drop is positioned in the Cassie–Baxter state, where its energy is minimized as compared to Wenzel mode. The variation of energy calculated from Eq. 4 must thus be weaker than that calculated from Eq. 2, from where:

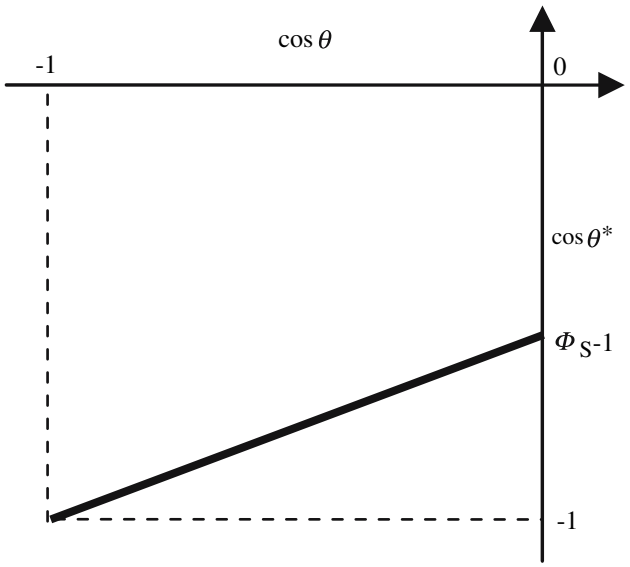

Fig. 9 Apparent contact angle according to the angle of Young (Cassie–Baxter relation)

$$\cos\theta_C = \frac{\phi_S - 1}{r - \phi_S} \quad (6)$$

This leads to a coexistence of the two modes, as described in Fig. 10:

However, when a drop is deposited on a rough surface, a Cassie–Baxter regime occurs even when $\theta < \theta_c$ (for water, $\theta < 120°$) [27–29]. This state is metastable, i.e. by applying a pressure to the drop, for example, it is possible to reach the Wenzel regime: stable and displaying an important hysteresis [30]. This state is problematic, in particular in microfluidic microsystems where the displacement of a drop with a hysteresis of 100° is not easily realizable. An ideal configuration is the *rolling ball* or *fakir* effect i.e. the Cassie–Baxter state.

Neinhuis and Barthlott studied in detail the superhydrophobic properties of almost 200 plants, the famous lotus effect. In most cases, the surface comprises two different roughness scales: one is micrometric and the other one is nanometric.

The first assumptions on this double roughness were brought by Bico [31], Herminghaus [32] and many other teams [33, 34]. According to the work of Bico, this double roughness would avoid placing the drop in the Wenzel state; small asperities will trap air and as a consequence the drop will be in an intermediate configuration between Wenzel and Cassie–Baxter [21] (Fig. 11).

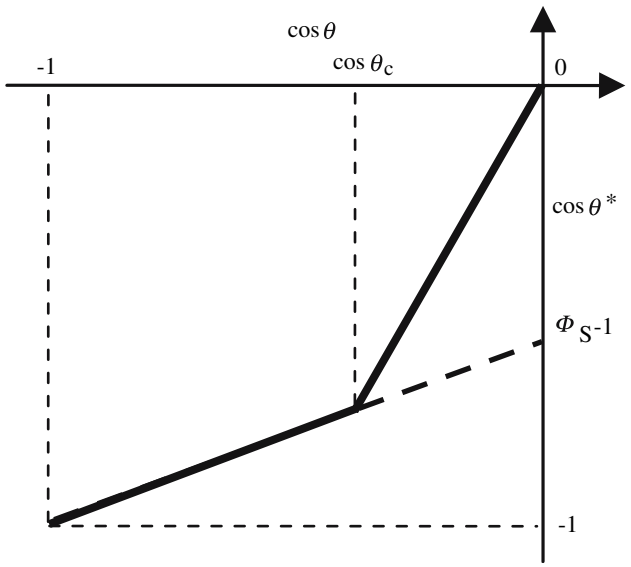

Fig. 10 Coexistence of two superhydrophobic modes. With feeble hydrophobicity (cos θ_c < cos θ < 0), the apparent contact angle is theoretically given by the relation of Wenzel while for strong hydrophobicity (cos θ < cos θ_c), the apparent contact angle follows the relation of Cassie–Baxter. However, in practice, an average hydrophobicity generally involves a metastable configuration of Cassie–Baxter (dotted lines)

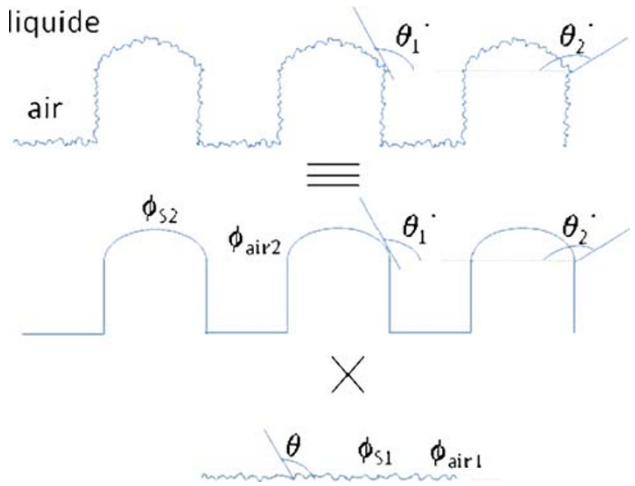

Fig. 11 Apparent contact angle on a surface with two different roughness scales

In the case of a double roughness, the equation of Cassie–Baxter becomes:

$$\cos\theta_2^* = \phi_{S1}\phi_{S2}\cos\theta - \phi_{S2}\phi_{A1} - \phi_{A2} \quad (7)$$

with

$$\cos\theta_2^* = \phi_{S2}\cos\theta_1^* - \phi_{A2} \quad (8)$$

and

$$\cos\theta_1^* = \phi_{S1}\cos\theta - \phi_{A1} \quad (9)$$

where θ is the angle of Young, θ_1*, Φ_{s1} and Φ_{A1} are respectively the angle, the solid fraction of surface and the fraction of air surface with nanometric roughness, and θ_2*, Φ_{s2} and Φ_{A2} are respectively the angle, the solid fraction of surface and the fraction of air surface with micrometric roughness (Fig. 11). From Eq. 7, the double roughness amplifies the superhydrophobic surface property. If, for example, two roughnesses are homothetic, they have the same fraction of surface Φ_s and the equation of Cassie–Baxter becomes:

$$\cos\theta^* = -1 + \phi_S^2(1 + \cos\theta) \quad (10)$$

When $\Phi_s < 1$, cos θ* is smaller than in the case of a simple roughness, the contact angle increases.

Preparation of Superhydrophobic Surfaces

From a technological point of view, there are currently several possibilities to mimic and prepare artificial superhydrophobic surfaces, including generating of rough surfaces coated with low surface energy molecules, roughening the surface of hydrophobic materials, and creating well-ordered structures using micromachining and etching methods. Some examples will be seen in the next part of this review.

Wettability Switching Techniques on Superhydrophobic Surfaces

Carbon Nanotubes Anisotropic Structures

Carbon nanotubes (CNTs) are naturally hydrophilic. However, their wetting behavior is highly dependent on their arrangement and can vary from hydrophilic to hydrophobic and even superhydrophobic with in addition isotropic to anisotropic CA hysteresis. Two strategies have been developed to reach a stable superhydrophobic state. First a chemical modification of CNTs with a low surface energy compounds [mainly fluoropolymers like poly(tetrafluoroethylene) and silanes] leading to a CA as high as 171° with a roll off behavior, consistent with a quasi null hysteresis [35]. Second, hierarchical structures inspired by the 'lotus effect' were fabricated by CVD on a patterned quartz substrate, giving a CA of 166° with a CA hysteresis of 3°. Using an anisotropically rough surface, leading to an anisotropic CA, Jiang et al. have prepared a surface mimicking the rice leaf (a two dimensional anisotropy) showing that a droplet can roll along a determined direction [36]. As predicted by Jiang [37], three-dimensional anisotropic structured carbon nanotubes (ACNTs) can be designed with a gradient roughness distributed in a particular direction where the gradient wettability is predetermined and therefore the droplet may move spontaneously, driven by the wettability difference.

Mechanical

The first report on a switching wettability based on roughness modification by mechanism action was proposed by He [38]. The device consists of a thin polydimethylsiloxane (PDMS) membrane bound on a top of rough PDMS substrate. The switching was dynamically tuned from medium hydrophobic to superhydrophobic states by deflecting the membrane with a pneumatic method. The flat surface shows a contact angle of 114.6° while for the rough surface containing square pillars (26×24 μm^2 with a 25 μm height, giving rise to superhydrophobic classical droplet behavior), the CA is about 144.4°. Pneumatic actuation of the membrane leads to a CA difference of 29.8° (from flat to rough surface) (Fig. 12). The droplet displacement is only possible across the boundary of the patterned area: the droplet is gently deposited on the rough surface (i.e. after actuating the membrane) and moves to the flat one: receding angle on the rough surface is greater by 17° than the advancing angle on the flat surface. This contact angle difference can generate enough driving force to produce droplet motion from rough to flat surface. However, the droplet did not move for a

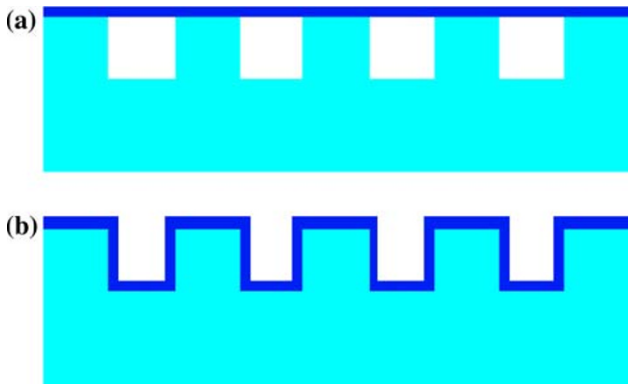

Fig. 12 Concept of the thin membrane device: (**a**) with a flat surface, (**b**) pneumatic actuation leading to a rough surface

reversible operation sequence (i.e. deposited on the flat surface then actuating the membrane). The authors explained the phenomenon by the formation of a wetted contact leading to a contact angle close to that on the flat surface. The driving force is not enough to cause droplet motion. A solution proposed by the authors to overcome this problem is to realize a double roughness of the surface in order to mimic superhydrophobic structures leaves.

Chen et al. [39] reported on the modification of surface wetting induced by morphology change (SWIM). A conductive metal/polymer composite membrane, supporting hydrophobic microposts of various heights, is sustained by negative photoresist spacers (Fig. 13). Before applying an electrical potential (initial state) a droplet is bolstered on the higher microposts with a contact angle of 152°. When a voltage (250 V) is applied between the conductive polymer membrane and the bottom addressable electrodes (actuated state), the membrane is bent (10 μm vertical displacement) due to the electrostatic force, and the highest microposts are lowered down. The droplet sticks to the lower posts and the contact angle decreases to 131°. Unfortunately, the authors did not indicate clearly the reversibility of the phenomenon, and did not precise the hysteresis observed for these surfaces. Nonetheless, an advantage of this mechanical device is a free electric interference mechanism compared to electrowetting and prevents the surface from nonspecific adsorption of proteins on the hydrophobic layer.

Zhang et al. [40] described a method to generate reversible wettability upon switching between superhydrophobicity and superhydrophilicity by biaxially extending and unloading an elastic polyamide film with triangular net-like structure composed of fibers of about 20 μm in diameter. The average side of the triangle of the net-like structure is around 200 μm before biaxial extending (with a CA of 151.2°) and 450 μm after extension (with a CA of 0 ± 1.2°) (Fig. 14). The mechanical actuation presented in this part consists mostly in increasing the liquid/solid surface (resulting in the modification of the apparent contact angle) rather than modifying directly the surface wetting properties.

Magnetic

A superhydrophobic surface was used for reversibly oriented transport of superparamagnetic microliter-sized liquid droplets with no lost volume in alternating magnetic fields. The surface consists of an aligned polystyrene (PS) nanotube layer prepared via a simple porous alumina membrane template covering method [41]. This surface displays a superhydrophobic behavior (CA of about 160°) with a strong adhesion force to water, as compared to traditional superhydrophobic surfaces. Instead of estimating the hysteresis of the surface, the authors measured the adhesive force. According to their results, adhesive forces of the surfaces were 10 times higher than that of a surface displaying a water CA hysteresis of 5°, proving the Wenzel state of the droplet. They used a super paramagnetic microdroplet (for an intensity of external magnetic field ranging from 0.3 to 0.5 T) placed on an ordinary superhydrophobic surface (CA of 160°), separated from the PS surface with 2 mm in height [42].

When the upper magnet was applied, the microdroplets were magnetized, fly upward and stick to the PS surface

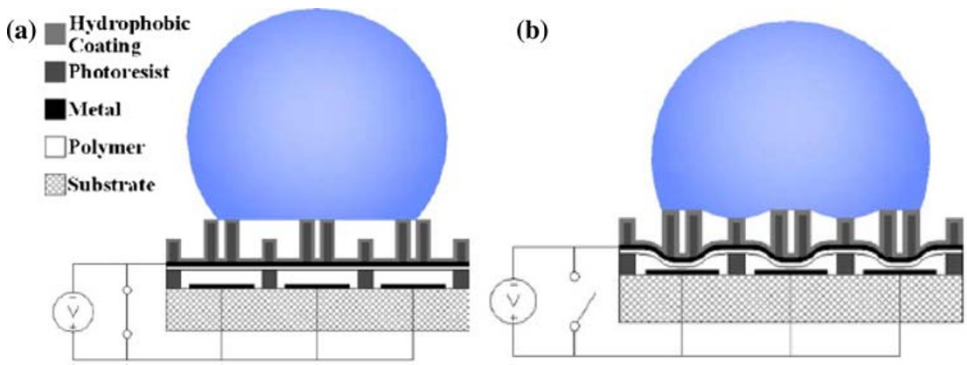

Fig. 13 The operation concept of SWIM: (**a**) at initial state, the droplet merely contacts the higher posts and (**b**) at actuated state, the droplet will contact with both the higher and lower posts. Reprinted with permission from [39]. Copyright 2007 Institute of Physics

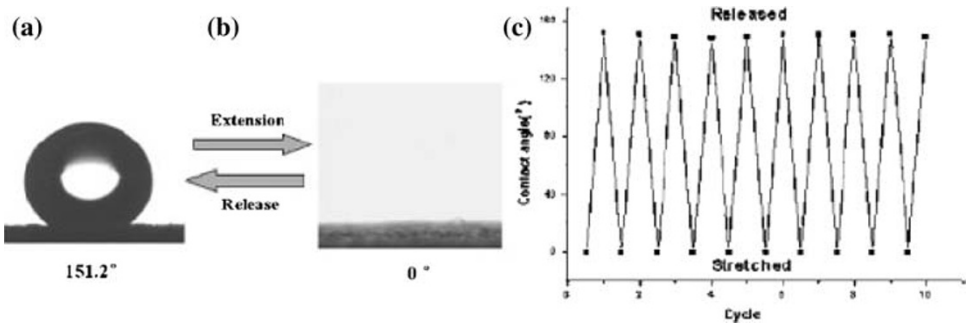

Fig. 14 Switching between superhydrophobicity and superhydrophilicity of an elastic polyamide film with a triangular net-like structure. (**a**) Before biaxial or after unloading, the CA is about 151°. (**b**) When the film was extended, the CA is around 0° (i.e. reversible superhydrophobic/superhydrophilic transition of the films by biaxial extension and unloading). Reprinted with permission from [40]. Copyright Wiley-VCH Verlag GmbH & Co. KGaA

due to its strong hysteresis. On the other hand, when the magnetic force was reversed, the microdroplet fell down onto the initial surface. The principal key point of this application is that the reversible transport is made without any lost of liquid.

Chemical

A two-level structured surface (SAS) of polymer has been synthesized by Zhou and Huch [43]. The first level of roughness ($\sim$1 μm) was obtained by plasma etching of a rough polymer film (PTFE). Then surface hydroxyl and amino functional groups have been introduced by plasma treatment in order to form a grafted mixed brush consisting of two carboxyl-terminated incompatible polymers PSF-COOH and P2VP-COOH. After exposure to toluene, an advancing contact angle of 160° was measured with no angle hysteresis (rolling ball state). After immersion of the sample in an acid (pH 3) bath for several minutes and its subsequent drying, a drop of water spreads on the surface. The authors clearly indicate that the superhydrophobic state is time dependant. Up to a few minutes after exposure to toluene, the surface was superhydrophobic with quasi null hysteresis, while the hysteresis increases dramatically with time due to the slow switching of the surface composition to a more hydrophilic state.

Temperature

The first demonstration on thermal reversible switching behavior between superhydrophilicity and superhydrophobicity was reported by Sun et al. [44]. They used a thermo responsive polymer poly(N-isopropylacrylamide) (PNIPAAm) that exhibit, when deposited on a flat surface, a CA modification from 63.5° for a temperature of 25 °C (hydrophilic state due to the formation of intermolecular hydrogen bonding between PNIPAAm chains and water molecules) to 93.2° at 40 °C (hydrophobic state due to intramolecular hydrogen bonding between C=O and N–H groups of the PNIPAAm chains). The roughness effect on the wetting properties was further investigated by depositing the polymer on rough surfaces (obtained by a laser cutter on a silicon wafer) formed of a regular array of square silicon microconvexes (grooves of about 6 μm width, 5 μm depth and spacing from 31 to 6 μm). The obtained results clearly show that when the substrate is sufficiently rough (i.e. when groove spacing is smaller or equal to 6 μm), the thermally responsive switching between superhydrophilicity and superhydrophobicity can be realized: from a CA of 0° below T = 29 °C to 149.5° above 40 °C, indicating that a combination of the change in surface chemistry and surface roughness can enhance stimuli-responsive wettability.

Fu et al. [45] have developed a slightly different approach based on porous anodic aluminum oxide (AAO) template with nominal pore sizes from 20 to 200 nm. The grafting of PNIPAAm on the template was obtained by surface-initiated atom transfer radical polymerization (ATRP) leading to a reproducible and uniform brush film (15 nm thick) on the textured surface. According to the authors, the macroscopic wettability is not due only to the change of the polymer hydrophobicity, but also to the nanoscopic topography of the surface associated with expansion and contraction of the grafted polymer. Nonetheless, these surfaces led to a maximum contact angle of 158° at 40 °C (for 200 nm pore size) starting from a CA of 38° at 25 °C, comparable to the contact angles reported by Sun et al. [44].

Dual Temperature/pH

Xia et al. [46] have prepared a dual-responsive surface (both temperature and pH) that reversibly switches

between superhydrophilic and superhydrophobic. In addition, the lower critical solubility temperature (LCST) of the copolymer is tunable with increasing the pH. The copolymer thin film is a poly(*N*-isopropyl acrylamide-co-acrylic acid) [p-(NIPAAm-co-AAC] deposited on a roughly etched silicon substrate composed of patterned square pillars (20 μm high, 12 μm long, and 6 μm spacing between the silicon pillars). For a pH = 7, identical behavior, from superhydrophilic to superhydrophobic was obtained, as compared to classical PNIPAAm discussed above. However, for pH values of 2 and 11, the surfaces are superhydrophobic and superhydrophilic, respectively, whatever the temperature (Fig. 15). Another point is that, as compared to previously related reports on thermally responsive materials, the film can be hydrophobic at low temperature and hydrophilic at high temperature. These phenomena can be linked to the reversible change in hydrogen bonding between the two components (NIPAAm and AAc). It is to be noted that the transformation from superhydrophobic to superhydrophilic takes several minutes (time for a single cycle).

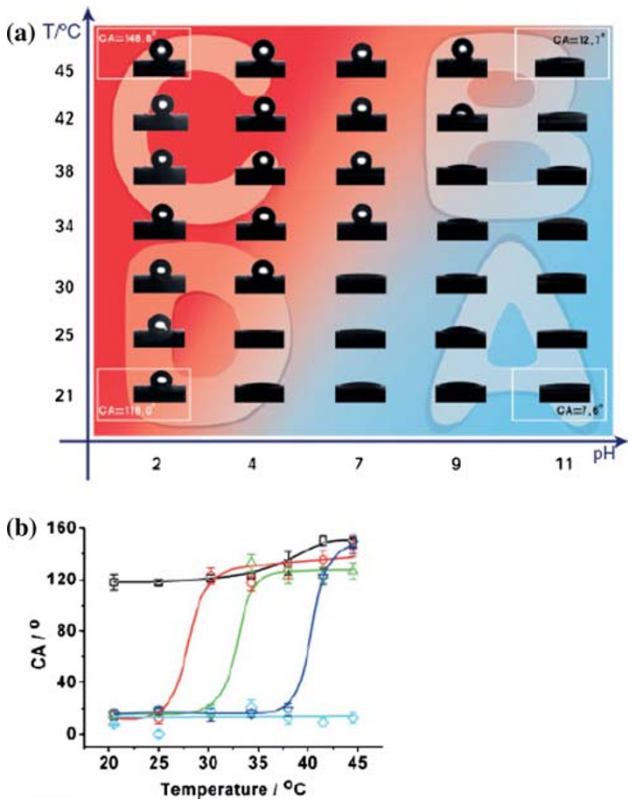

Fig. 15 (**a**) When the pH and/or temperature is varied the CAs reversibly change. (**b**) Temperature and pH dependence of water CAs for P(NIPAAm-co-AAc) thin films. Water CAs change at different temperatures for a modified substrate at pH values of 2 (□), 4 (○), 7 (▲), 9 (▼) and 11 (◇), respectively. Reprinted with permission from [46]. Copyright Wiley-VCH Verlag GmbH & Co. KGaA

Optical

The first example showing that the wetting characteristics of polymer surfaces doped with photochromic spiropyran molecules can be tuned when irradiated with laser beams of properly chosen photon energy was reported by Athanassiou et al. [47]. The hydrophilicity was enhanced upon UV laser irradiation since the embedded nonpolar spiropyran molecules were converted to their polar merocyanine isomers. The process is reversed upon green laser irradiation. To enhance the hydrophobicity of the system, the photochromic polymeric surfaces were structured using soft lithography. Water droplets on the patterned features interact with air trapped in the microcavities, creating superhydrophobic air–water contact areas. Furthermore, the light-induced wettability variations of the structured surfaces are enhanced by a factor of 3 compared to those on flat surfaces. This significant enhancement is attributed to the photoinduced reversible volume changes of the imprinted gratings, which additionally contribute to the wettability changes induced by the light. In this work, it was demonstrated how surface chemistry and structure can be combined to influence the wetting behavior of polymeric surfaces. However, the contact angle values after the UV and green light irradiation are limited to the first two UV–green irradiation cycles. The aging and degradation of the system upon multiple irradiation cycles is the major drawback of such a polymeric system.

On the other hand, Lim et al. [48] have reported a photoswitchable nanoporous multilayer film with wettability that can be reversibly switched from superhydrophobicity to superhydrophilicity under UV/visible irradiation. They used a combination of surface roughness and a photoresponsive molecular switching of fluorinated azobenzene molecule (7-[(trifluoromethoxyphenylazo)phenoxy]pentanoic acid (CF3AZO)). The surface roughness was obtained using a layer-by-layer deposition technique of poly(allylamine hydrochloride (PAH)), which is a polyelectrolyte, and SiO_2 nanoparticles as polycation and polyanion, respectively giving a porous organic–inorganic hybrid multilayer films on silicon surface. In their study, the surface roughness can be precisely tuned by controlling the number of PAH/SiO_2 NPs bilayers. The film was further modified by 3-(aminopropyl)triethoxysilane to introduce amino groups serving as binding sites for the photoswitchable moiety. The wettability is dependent on the change of the dipole moment of the azobenzene molecules upon *trans* to *cis* photoisomerization (Fig. 16). For example, in the *trans* state, the azobenzene molecules exhibit the fluorinated moiety leading to a lower surface energy. The *trans*-to-*cis* isomerization of azobenzene is induced by UV light irradiation and leads to a large increase in the dipole moment of these molecules demolishing the chain packing in the azobenzene

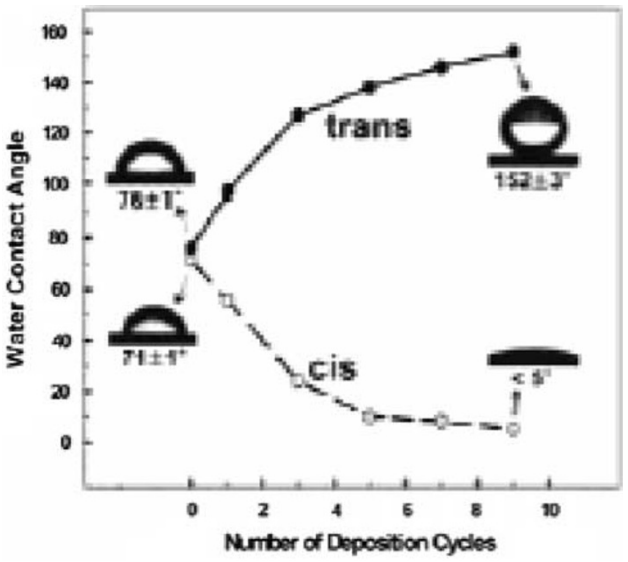

Fig. 16 The relationship between the number of deposition cycles and the water contact angles: water droplet profiles on the smooth substrate (dotted arrows) and on the organic/inorganic multilayer film (solid arrows) after UV/visible irradiation. Reprinted with permission from [48]. Copyright 2006 American Chemical Society

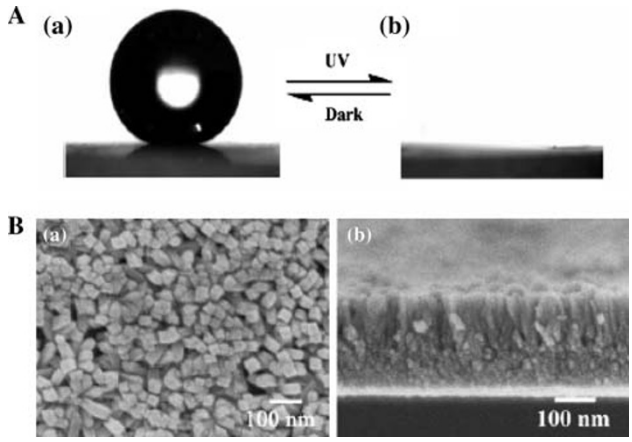

Fig. 17 (A) Water droplet shapes on as-prepared SnO_2 nanorod films (**a**) before and (**b**) after UV-irradiation; (B) (**a**) and (**b**) are the top and cross-sectional FE-SEM images of the as-prepared SnO_2 nanorod films, respectively. Reprinted with permission from [49]. Copyright 2007 Royal Society of Chemistry

monolayer and a lower contact angle (the fluorinated moiety was not anymore exhibited). By this technique, the contact angle can be controlled by adjusting the number of multi-electrolyte layers. A contact angle of 152° and a hysteresis below 5° was obtained for 9 bilayers with a little degradation after many cycles. They showed that patterning surface with hydrophilic and superhydrophilic zones can be easily achieved by using selective UV irradiation through an aluminum mask.

The photoswitchable wettability of aligned SnO_2 nanorod films was demonstrated by Zhu et al. [49]. The SnO_2 nanorod films were prepared in two steps. First, SnO_2 seeds were spin-coated on a silicon substrate and then immersed in 50 mL aqueous solution of $SnCl_4 \cdot 5H_2O$ in the presence of urea and HCl in a closed bottle. The mixture was heated at 95 °C for 2 days to yield SnO_2 nanorod films. The resulting films were rinsed thoroughly with deionized water, dried at room temperature and stored in the dark for several weeks. The as-prepared SnO_2 nanorod films showed superhydrophobic behavior (contact angle of 154°), as compared to 20° displayed by a smooth SnO_2 surface. SnO_2 nanorod films changed to superhydrophilic state (0°) just by exposition to UV irradiation (254 nm) for 2 h. Then, the wettability goes back to its initial superhydrophobic state by keeping the films in the dark for a given time (4 weeks) [49] (Fig. 17). The switchable wettability was explained by the generation of hole-electron pairs after UV-irradiation on the surface of the SnO_2 nanorods reacting with lattice oxygen to form surface oxygen vacancies. The defective sites are kinetically more favorable for hydroxyl adsorption than oxygen adsorption, leading to the superhydrophilic state. During dark storage, hydroxyls adsorbed on the defective sites can be gradually replaced by oxygen in the air, because oxygen adsorption is thermodynamically more stable and lead to superhydrophobic state. Feng et al. showed similar switchable wettability properties for ZnO nanorod films [50]. In these cases, the reversible switching between superhydrophilicity and superhydrophobicity is related to the cooperation of the surface chemical composition and the surface roughness. The former provides a photosensitive surface, which can be switched between hydrophilicity and hydrophobicity, and the latter further enhances these properties.

By using titania nanoparticles, a patterning and tuning method of microchannel surface wettability was developed for microfluidic control [51]. Titania modification of a microchannel was achieved by introduction of titania solution inside pyrex microchannel providing a nanometer-sized surface roughness. Subsequent hydrophobic treatment with ODS (octadecyl dichlorosilane) gavelled to superhydrophobic surface (contact angle of 150°). Photocatalytic decomposition of the coated hydrophobic molecules was used to pattern the surface wettability, which was tuned from superhydrophobic to superhydrophilic under controlled photoirradiation (Fig. 18). Irradiation for 60 min gave a superhydrophilic surface (9°). This wettability changes were explained by the small number of ODS molecules covering the titania surface caused by photocatalytic decomposition of ODS. Furthermore, a four-step wettability based Laplace valves working as passive stop valves were prepared by using the patterned and tuned surface. As a demonstration, a batch operation system consisting of two sub-nL dispensers and a reaction

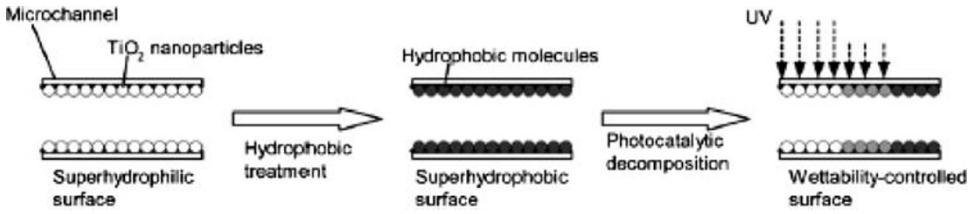

Fig. 18 Photocatalytic patterning and tuning of surface wettability by photoirradiation of modified titania nanoparticles. Reprinted with permission from [51]. Copyright 2007 Royal Society of Chemistry

chamber was constructed. Fundamental liquid manipulations required for the batch operation were successfully conducted, including liquid measurement (390 and 770 pL), transportation, injection into the chamber, and retention in the chamber. To verify the quantitative operation, the system was applied to a fluorescence quenching experiment as an example of volumetric analyses. The method provides flexible patterning in a wide range of tuned wettability surfaces in microchannels even after channel fabrication and it can be applied to various two- or multi-phase microfluidic systems.

Another example of titanium-based material was described by Balaur et al. [52]. They used self-organized TiO_2 nanotube layers grown on Ti by electrochemical anodization. The as-prepared TiO_2 nanotubes displayed a superhydrophilic wetting behavior. When modified with organic molecules, such as octadecylsilane or octadecylphosphonic acid layers, the surfaces showed a superhydrophobic behavior. They have demonstrated how the tubular geometry of the TiO_2 layers combined with an irreversible UV induced decomposition of the organic monolayers can be used to adjust the surface wetting properties to any desired degree from super-hydrophobic to superhydrophilic (Fig. 19).

Nanowires can also be used for the preparation of superhydrophobic surfaces with a tunable wettability. Coffinier et al. presented a simple method for producing superhydrophobic surfaces based on chemical modification of silicon oxide nanowires [53]. Nanowires with an average mean diameter in the range of 20–150 nm and 15–20 μm in length were obtained by the so-called solid–liquid–solid (SLS) mechanism at 1,100 °C under N_2 flow during 60 min. The porous nature and the high roughness of the resulting surfaces were confirmed by AFM imaging. After cleaning, the silicon nanowires have been modified by PFTS (perfluorodecyl trichlorosilane), resulting in a superhydrophobic surface with a contact angle of 152°, which is much higher than that of a smooth Si/SiO_2 surface modified with the same silane (109°) (Fig. 20). The contact angle of the unmodified surface was closed to 0°, as expected for a surface terminated with polar hydroxyl (OH) groups. The surface wettability can be irreversibly tuned by controlling the UV-irradiation time, resulting in a partial or complete removal of the organic layer. The chemical modification and degradation of the organic layer was followed by XPS analysis.

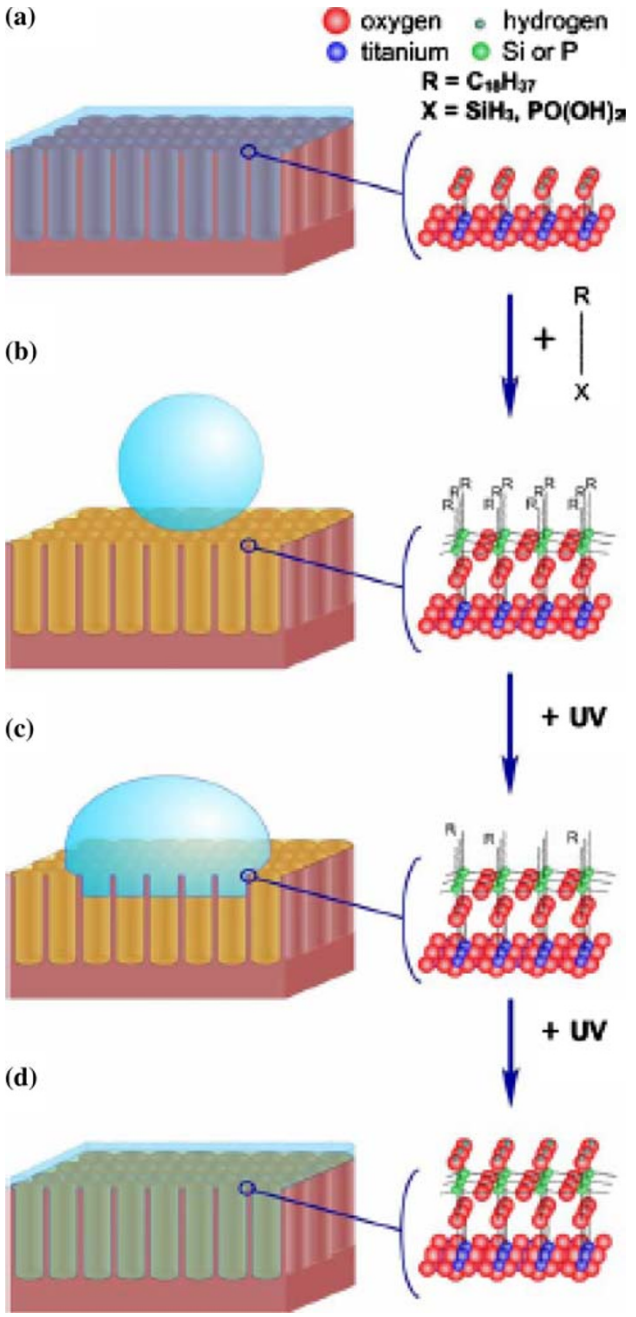

Fig. 19 Schematic illustration of the process used to adjust contact angles. The scheme shows the different stages of the wetting behavior: (**a**) the nanotube surface; (**b**) superhydrophobicity after hydrophobic modification; (**c**) chain scission of the organic layer triggered by UV light and (**d**) leading finally to complete wetting. Reprinted with permission from [52]. Copyright 2005 Elsevier

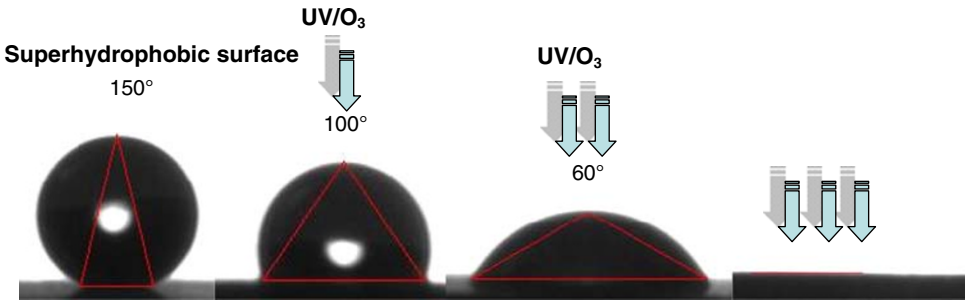

Fig. 20 Control of wettability of PFTS-terminated silicon oxide nanowires as a function of exposition time to UV-irradiation

EWOD

Theory and History

Lippmann showed, during his thesis on electrocapillarity in 1875 [54], that the application of a voltage between an electrolyte and a drop of mercury immersed in this one involved the creation of a double electric layer (EDL, Electric Double Layer) at the interface. The electrowetting principle consists, starting from the electrocapillarity phenomenon, to modify the shape of a liquid droplet placed on a surface during the application of a voltage (Fig. 21). Since the majority of the liquids used in Lab-on-Chip devices are conductive, the idea developed by Berge was to isolate the drop from the substrate using a dielectric layer in order to avoid any phenomenon of electrolysis [55]. This development is known as ElectroWetting On Dielectric (EWOD).

The system can be seen like a variable capacitor [56]. The energy stored in this capacitor according to a direction perpendicular to the plan, noted $W(x)$, is expressed by:

$$W(x) = \frac{1}{2}C(x)V^2 = \frac{\varepsilon_0\varepsilon_r}{2e}xV^2 \tag{11}$$

where ε_r is the permittivity of the dielectric layer, ε_0, the electric permittivity of the vacuum, x, the length of the capacitor and E, its thickness. By applying the principle of virtual work, the force per transverse unit of length is deduced:

$$F_m = \frac{\partial W(x)}{\partial x} = \frac{\varepsilon_0\varepsilon_r}{2e}V^2 \tag{12}$$

This force, acting on the three phase contact line, can be inserted in the equation of Young (**1**):

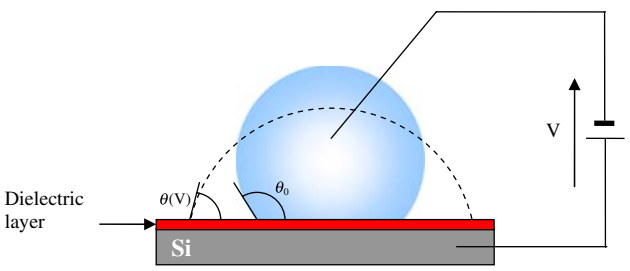

Fig. 21 EWOD principle. Under applied voltage, the drop spreads out on the surface

$$\gamma_{LS} = \gamma_{SG} - \gamma\cos\theta(V) + \frac{\varepsilon_0\varepsilon_r}{2e}V^2 \tag{13}$$

Equation 1 leads then to the equation of Young–Lippmann established by Bruno Berge in 1993:

$$\cos\theta(V) = \cos\theta_0 + \frac{\varepsilon_0\varepsilon_r V^2}{2\gamma e} \tag{14}$$

Although, Young–Laplace pressure works in prediction of droplet shape modification by EWOD, different theories have been proposed to explain the real nature of the movement. Historically, electrowetting was explained by the variation of interfacial energies: the increase of the voltage leads to a solid–liquid interfacial energy diminution [57]. More recently, it has been proved that EWOD can be interpreted as an electromechanical effect: pressure exerted by electrical field on the drop surface acts on the contact line [58–60]. While this last view seems to be the correct one, both of them predict the same contact angle variation [61, 62].

Furthermore, according to Eq. 14, it is theoretically possible to obtain a total wetting of the drop by increasing the applied voltage. However, a saturation of the contact angle is observed starting from a certain voltage. The literature brings many assumptions for the comprehension of this saturation like an increase in the electric field to the level of the three phase contact line due to pick effect [63], trapping of charges in or on the dielectric layer [64, 65], ionization of air on the level of the triple line [66], leakage on the dielectric layer, [67]. Nevertheless, while reasons for this saturation are not clearly established by the scientific community, in practice the maximum tension V_{max} to be applied for electrowetting is always observed.

Optical Applications of EWOD

This part of the review, which is not exhaustive deals with the potential applications of the EWOD technique. For more detailed state of the art as well from the theoretical point of view, refer to recent reviews by Mugele and Baret [68] (which in addition contains an English version of the thesis of Lippmann on electrocapillarity), and by Fair [69].

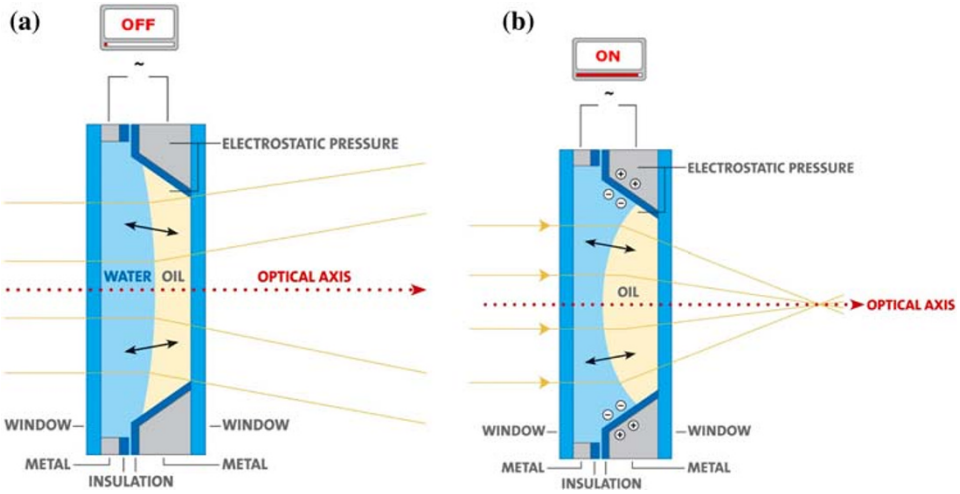

Fig. 22 Principle of Varioptic liquid lenses operation based on EWOD principle: (**a**) the tension is cut off, the rays are divergent, (**b**) the tension is applied, the rays are focalized [71]. Reprinted with permission from Varioptic

Berge was the first to bring a microsystem based on EWOD to maturation at the industrial level with liquid lenses [70]. The principle is simple and is schematically represented in Fig. 22. Oil and water drops are trapped between two transparent substrates. The spacing between the two substrates is ensured by metal electrodes. At V = 0 V, the drops form a certain contact angle with the surface. The formed meniscus thus has a defined radius of curvature, and optical rays are divergent (Fig. 22a). Upon application of a tension of ~60 V, the contact angle changes, the radius of curvature is modified, the luminous rays are focused (Fig. 22b).

Figure 23 exhibits two models of lenses. The market aims primarily that of mobile telephony. Recently, Varioptic commercialized its first autofocus module, in partnership with Sunny Optics (China). These lenses have several advantages, as compared to the traditional lenses. First of all, the absence of moving parts allows a better integration. The weak voltage required for actuation allows the introduction of autofocus modules into the mobile telephones. Lastly, the lens has a perfect surface since it is about the interface between two liquids with a price divided by 10.

Fig. 23 Two models of lenses developed by Varioptic. Reprinted with permission from Varioptic

Several teams work on the development of such lenses. The principal stake is the reduction of the tension, necessary to the operation of the lens. The team of Heikenfeld at the University of Cincinnati developed a concept of optical prism by obtaining flat meniscuses for a drop taken between two substrates [72]. By applying a specific tension to each substrate, it is possible to vary the orientation of the prism (Fig. 24) [73].

EWOD allows also visualizing images thanks to screens containing liquid pixels controlled by electrowetting. A spin-off of Philips, Liquavista [74], develops color screens based on electrowetting. The market aimed with such screens is always that of mobile telephony. The principle is similar to that of the Varioptic lenses. Each pixel consists of a water drop, which lets pass the light, and of an oil drop, opaque or of color. If no voltage is applied, the oil drop spreads out, the light does not go through (or the pixel is colored). On the other hand when a voltage is applied, the water takes the place of the oil, resulting in a white

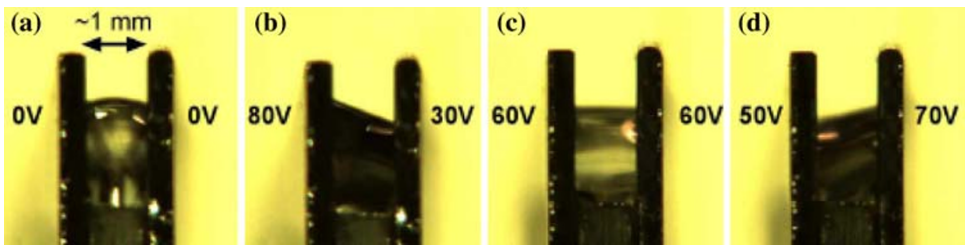

Fig. 24 Response of the prisms according to the applied voltage to each substrate. Reprinted with permission from [73]. Copyright 2006 Optical Society of America

pixel [75]. A general diagram of a monochromic and fluorescent pixel is presented in Fig. 25 [76]. In the case of the pixel developed at the University of Cincinnati by Heikenfeld, the principle is the reverse. The pixel is fluorescent if no voltage is applied (fluorescent oil for λ = 405 nm). Once a voltage is applied, the water takes the place of the oil and the light is completely reflected, the pixel is extinct.

EWOD for Microdroplets Displacement

In order to displace microdroplets and to realize microfluidic basic operations (merging, creating droplets), the EWOD system needs to have two plans: a base composed of electrodes for displacement and a counter-electrode (instead of a needle). A general diagram of the two plans microsystem is shown in Fig. 26. Initially, no voltage is applied between the electrodes and the counter-electrode, and whatever the place where the drop is placed, the contact angle is the contact angle of the drop θ_0. When a voltage is applied on an electrode under the drop, the contact angle of the three phase contact line in contact with this electrode decreases to reach a value θ_d and thus the radius of curvature R_d of the meniscus increases. The contact angle on the rest of the substrate is always the contact angle to balance θ_0 and the associated radius of curvature R_0 is lower than the radius of curvature R_d.

According to the Laplace law, the meniscus curvature radius change involves a difference in pressure within the drop [77]. This pressure difference is given by:

$$\Delta P = P_g - P_d \tag{15}$$

where P_g is the pressure on the left side in the drop whereas P_d is the pressure on the right side. These two values are determined by the following expressions:

$$P_g - P_a = \gamma\left(\frac{1}{R_0} + \frac{1}{R}\right) \tag{16}$$

$$P_d - P_a = \gamma\left(\frac{1}{R_d} + \frac{1}{R}\right) \tag{17}$$

where P_a is the atmospheric pressure, R the ray of the drop in the transverse direction, R_0, the radius of curvature of the left meniscus and R_d, the radius of curvature of the right meniscus. Thus,

$$\Delta P = \gamma\left(\frac{1}{R_0} - \frac{1}{R_d}\right) > 0 \tag{18}$$

The pressure within the drop is stronger on the left than on the right, the drop moves on the electrode of right-hand side. So with:

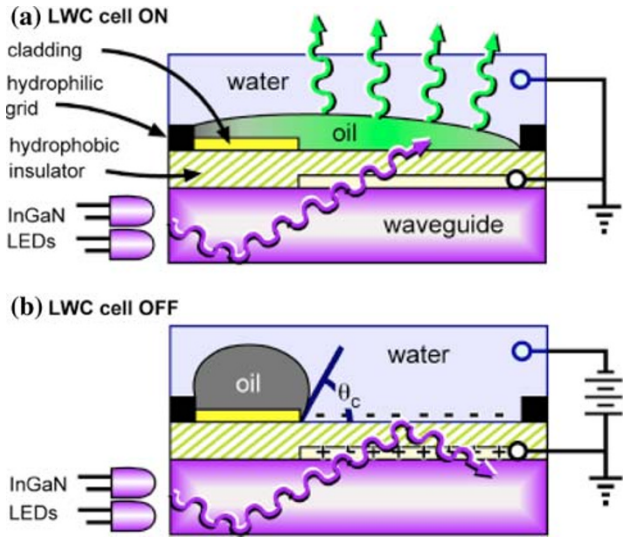

Fig. 25 General diagram of the liquid pixel for fluorescent screen produced at the University of Cincinnati. Reprinted with permission from [76]. Copyright 2005 American Institute of Physics

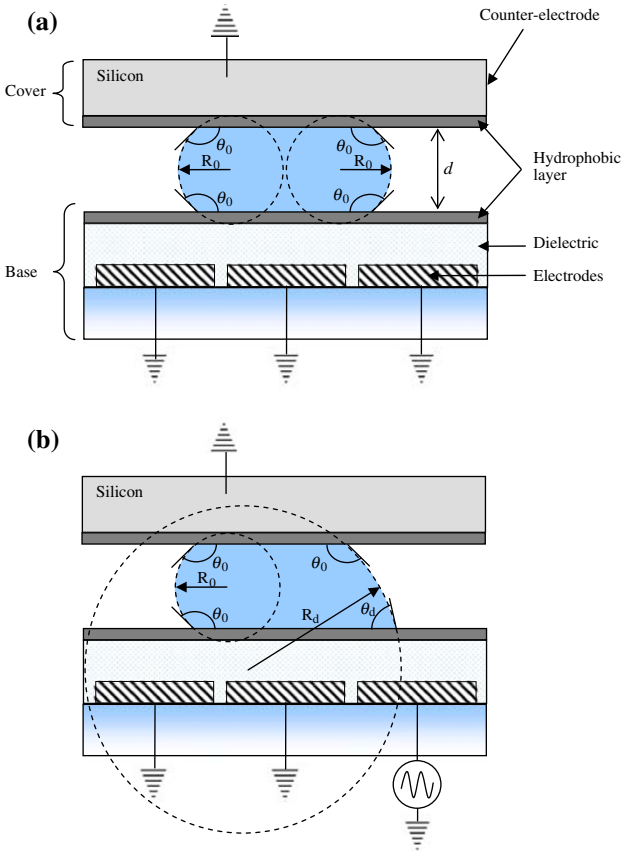

Fig. 26 General set up of an EWOD microsystem for the displacement of microdroplets: (**a**) no voltage is applied to the electrode, (**b**) a voltage is applied to the electrode of right-hand side

$$R_0 = -\frac{d}{2\cos\theta_0}$$

$$R_d = -\frac{d}{\cos\theta_0 + \cos\theta_d}$$

We found:

$$\Delta P = \gamma \frac{\cos\theta_d - \cos\theta_0}{d} \quad (19)$$

Starting from Eq. 19, the driving force F_m, which allows displacement, can be deduced (per unit of length):

$$F_m = \gamma(\cos\theta_d - \cos\theta_0) \quad (20)$$

The force F_m drives the drop on the electrode under applied voltage. Until now, all the calculations were applied for perfect surfaces. However, certain forces such as hysteresis or viscous forces can hinder the displacement of the drop. Fouillet showed by digital simulation that the movement of the drop is related to the interfacial forces and not to the viscous forces [78]. Concretely, it is necessary that the driving force is higher than the force of hysteresis in order to obtain a displacement of the drop. Within the framework of real surfaces, it is thus necessary that the driving force is higher than the force of hysteresis.

Lab-on-chip Applications

Although the industrial applications of the EWOD are in the field of optics, several groups are also interested in the possible applications in biotechnology. For this purpose, it is necessary to displace biological liquids and to realize microfluidic elementary operations for the development of Lab-on-chip, LoC. The LoC based on EWOD were initiated by Pollack et al., from the Duke University [79, 80]. By carrying out a series of electrodes, it is possible to move by EWOD effect the drop from one electrode to its neighbor by successive polarization. In this case, the electrodes are made of chromium; the dielectric is parylene C (700 nm thick) covered with Teflon (200 nm thick). The counter-electrode is a covered blade of glass ITO and Teflon. The gap between the two substrates is 300 μm for electrodes of 1.5 mm^2. The displacement of drops of KCl (100 mM) was carried out under a tension of 120 V_{DC}. In 2004, the same team has developed a Lab-on-Chip based on EWOD allowing the determination of the concentration of glucose in a drop of plasma, serum, urine and saliva [81]. The detection scheme was based on the change of absorbance of the sample mixture/reactive versus time.

Other Lab-on-Chip devices have been realized by research teams from the University of Los Angeles, USA and CEA-Grenoble, France. Kim and Garrell from the University of Los Angeles (UCLA) developed a device offering the possibility to carry out several operations, including MALDI mass spectrometry analysis [82]. A microsystem comprised of different zones for sample purification and MALDI analysis is illustrated in Fig. 27. The method consists in moving a drop of biological liquid containing peptides and other impurities (urea, salts) by electrowetting on a hydrophobic Teflon pad. Peptides are adsorbed on the surface by hydrophobic/hydrophobic interactions. A water drop, moved by EWOD, dissolves the impurities mixed with peptides. Finally, a drop of a matrix is brought on the pad and the microsystem is introduced into a MALDI mass spectrometer. At the same period, similar microsystems have been developed and patented within the framework of contract BIOCHIPLAB [83].

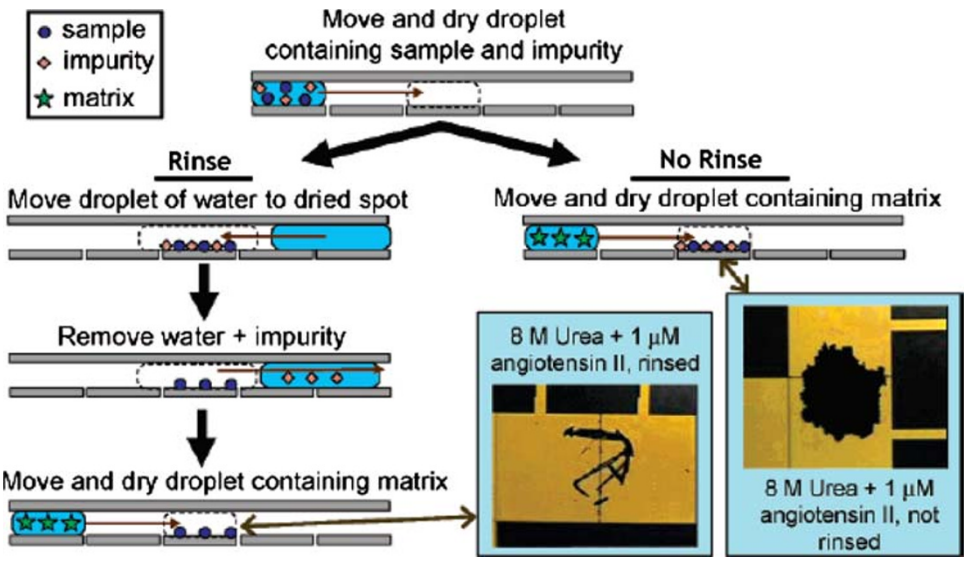

Fig. 27 Lab-on-Chip principle for MALDI mass spectrometry analysis developed by Kim and Garrell. Reprinted with permission from [82]. Copyright 2005 American Chemical Society

Discussion

The hysteresis effect and the saturation phenomenon limit the interval of tension to be used for EWOD. Concretely, the voltage allowing displacement must lie between V_{min} (related to hysteresis) and V_{max} (related to saturation). The microsystems have most of the time vocation to be embarked. It is thus necessary to reduce the tensions of actuation. One of the solutions is the development of 1 plan microsystems, i.e. without counter-electrode [84]. In this case, the force related to hysteresis is only reduced by a factor $\sqrt{2}$, which is still not very practical in an embarked system. Moreover, such microsystems are definitely more sensitive to evaporation and do not allow microfluidic operations like drop scission. Another solution consists to reduce the thickness of the dielectric layer or to increase the permittivity of this one. However, a reduction in the dielectric layer involves an increase in the electric field. Under a certain thickness, the electric field is higher than the dielectric rigidity and involves a breakdown of the layer. There is thus a limit in the reduction of tension. The increase in the permittivity of the dielectric layer is limited by the weak permittivity of the hydrophobic layer. Thus, there is a breakdown even when a voltage of only few volts was applied [63].

The last possibility is the reduction of the hysteresis by using superhydrophobic surfaces (with hysteresis lower than Teflon).

Nonreversible Electrowetting on Superhydrophobic Surfaces

Up to date, all the teams working on electrowetting on superhydrophobic surfaces encountered the same problem: a drop wedged in a nanostructure does not go up, leading to an irreversible EWOD effect. Several groups have tried for the last few years to obtain a reversible electrowetting phenomenon, but unsuccessfully. Krupenkin [85] from the Bell Lab (USA) is one of the precursors in this field. The surfaces employed in the study are composed of silicon pillars, engraved through a mask carried out by electronic lithography ('fakir carpet' geometry). The electric insulation is ensured through oxidation of the surface. Upon applying a voltage, a total damping of the drop on the surface was observed, as shown in Fig. 28. Unfortunately, this phenomenon proves to be irreversible.

The same group brings in 2005 a first solution for the reversible wetting on such surfaces [86]. A very short electrical current impulse applied to the substrate leads to the surface heating. The temperature can then reach 240 °C, causing liquid boiling and droplet expelling from the surface. Even though this technique is easy to implement, it is hard to imagine such an integrated system within a Lab-on-Chip. The heating would cause significant damage to biological material within the drop. Moreover, this expulsion creates satellite droplets.

Other teams worked on electrowetting on textured surfaces by using various materials, like SU-8 [87] or carbon nanotubes (CNT) [88]. In the first case, the reversibility is not total. The angle decreases from 152° to 90° under 130 V and returns back to 114° when the tension is cut off. In the second case (CNT), no reversibility is observed. A solution allowing the reversibility is to modify the ambient conditions. Indeed, the irreversibility is observed when the ambient condition is air. By replacing air by a hydrophobic medium, like oil (dodecane), it is possible to obtain reversibility as shown in the Fig. 29. The angle decreases from 160° to 120° (100° in air) when a tension was applied and returns back to 160° after tension cut off (Fig. 29).

It is interesting to notice that an oil environment prevents the Wenzel effect. However, the question of the

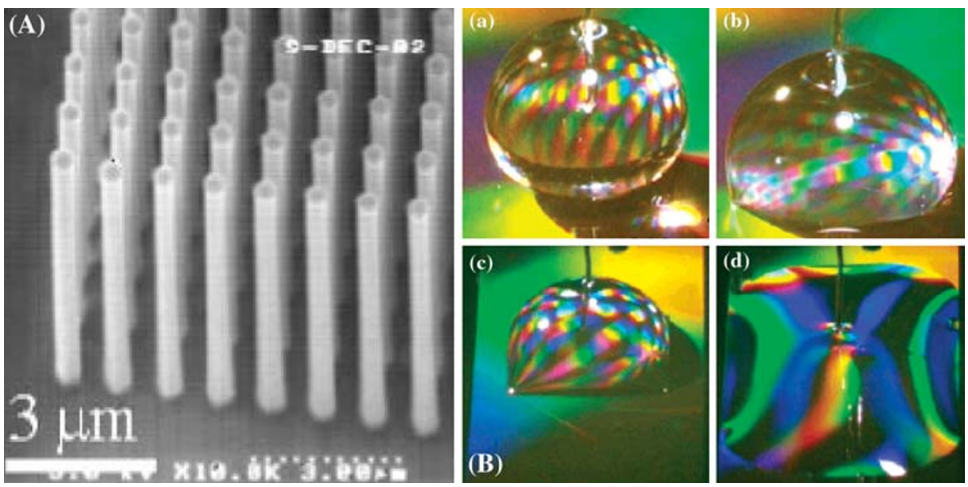

Fig. 28 (A) SEM image of the silicon nanostructure used for electrowetting, (B) total wetting by electrowetting of a drop of cyclopentanol on an e-beam nanostructured surface: (**a**) no tension is applied, (**d**) total wetting under application of a tension (50 V). Reprinted with permission from [85]. Copyright 2004 American Chemical Society

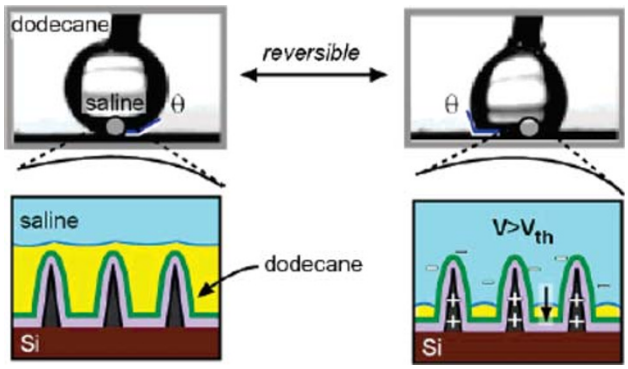

Fig. 29 Reversibility of EWOD phenomenon on superhydrophobic surface by immersion of the water drop in dodecane. Reprinted with the permission from [88]. Copyright 2006 American Chemical Society

applicability of such a surface is not clearly explained since a water drop in an oil environment has already a very high contact angle [89], even on a planar surface.

A fast calculation makes it possible to determine the angle of a water droplet on Teflon in an oil environment starting from the equation of Young:

$$\gamma_{ES} = \gamma_{SH} - \gamma_{EH} \cos\theta_0 \tag{21}$$

with

$$\gamma_{ES} = 47\,\mathrm{mN\,m^{-1}}$$

$$\gamma_{SH} = 2\,\mathrm{mN\,m^{-1}}$$

$$\gamma_{EH} = 50\,\mathrm{mN\,m^{-1}}$$

We found:

$$\theta_E = 154^\circ$$

Thus a planar surface allows at the same time a total wetting but also a complete reversibility.

Recently, Heikenfeld has reported electrowetting applied to textiles [90]. Two electrowetting textiles were prepared. The first one is made of a polyethylene naphthalate (PEN) film containing holes coated with Al (50 nm) (conductive layer). The second one was fabricated from wood microfibers on which a polymer (PEDOT-PSS and PEI) was deposited to render it electrically conductive. In both case parylene C (1 μm) and a fluoropolymer solution were used to insure a hydrophobic dielectric surface coating. The textile surfaces investigated are highly irregular and their electrowetting behavior was predicted, in first approximation by Cassie Baxter equation. For both textiles, irreversible electrowetting was observed with a contact angle varying from 120° to 70° in air. Here again, reversible electrowetting occurs in an oil environment.

Reversible Electrowetting on Superhydrophobic Surfaces

Our group has developed a different strategy to achieve electrowetting on superhydrophobic surfaces using a very heterogeneous surface composed of silicon nanowires coated with a fluoropolymer C_4F_8 [91]. The SiNWs were grown on Si substrate using the vapor–liquid–solid (VLS) mechanism and electrically insulated with 300 nm of SiO_2, First, a thin film of gold (4 nm thick) was evaporated on the substrate and then exposed to silane gas at different pressures at 500 °C for a given time. According to time and pressure of growth, eight surfaces were realized where the nanowires length varied from 1 μm (10 min, 0.1 T) to 30 μm (60 min, 0.4 T). Figure 30a shows a scanning electron microscopy (SEM) image of SiNWs grown at 0.1 T for 10 min. It consists of low density of SiNWs around 1 μm in length. High density of SiNWs with an average diameter in the range of 20–150 nm and 30 μm in length were obtained at 0.4 T for 60 min, leading to a nonuniform structured surface (Fig. 30b) Table 1.

To achieve surface superhydrophobicity, the SiNWs were coated with a fluoropolymer C_4F_8 (60 nm thick), deposited using a plasma technique. All the resulting surfaces displayed liquid contact angle θ^* around 164° for a saline solution (100 mM KCl) in oil (undecane) with almost no hysteresis, confirming that the droplet is in a Cassie state. Electrowetting in oil was performed on all

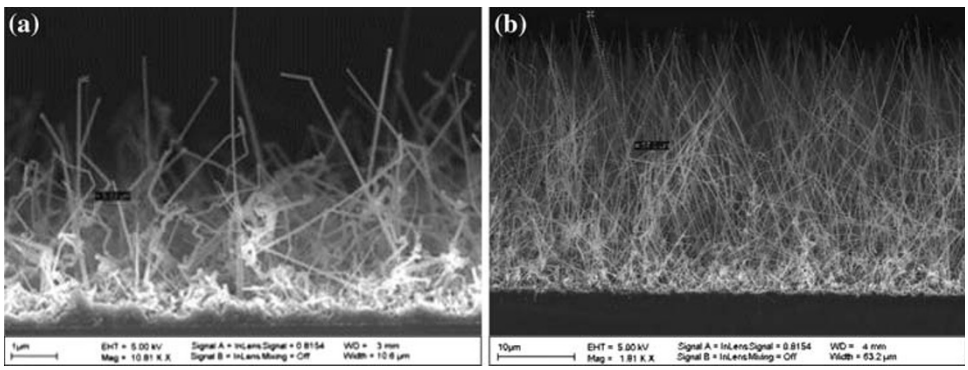

Fig. 30 SEM images of silicon nanowires grown on a silicon wafer coated with a thin gold layer (4 nm) at 500 °C (**a**) P = 0.1 T, (**b**) P = 0.4 T. The silane flow is of 40 sccm, the time of growth is 60 min

Table 1 Growth conditions of silicon nanowires (Q = 40 sccm, T = 500 °C)

No.	Time (min)	Pressure (T)	Length (μm)
1	10	0.1	1
2	10	0.4	1
3	20	0.1	2.5
4	20	0.4	15
5	40	0.1	8
6	40	0.4	35
7	60	0.1	7
8	60	0.4	30

surfaces, but a reversible behavior was only observed for the surface prepared using the process 8. When a voltage of 150 V_{rms} was applied, the apparent contact angle decreased down to 106° for a saline solution (100 mM KCl). When the tension was cut off, the effect is completely reversible. The drop returns to its initial position. Applied voltage leads to nonreversible wetting on the other surfaces (droplet trapped in a Wenzel configuration).

Same experiments have been carried out in air, on all the surfaces. Only the surface prepared using the process 8 allows a reversible electrowetting with electrowetting induced a maximum reversible decrease of the contact angle of 23° to reach 137° (starting from 160°). Turning off the voltage leads to a complete relaxation of the droplet (Fig. 31). This effect is ascribed to the high heterogeneity of the surface and trapped air under the droplet preventing to reach the Wenzel configuration [92].

We have shown for the first time that reversible electrowetting is possible on superhydrophobic surfaces that display specific geometrical criteria as predicted by Bico [24]. Due to low hysteresis of the surface, we assume that small voltages could be sufficient for droplet displacement. We have previously demonstrated the possibility to use such surfaces as EWOD ground electrodes with hydrophobic electrodes for matrix-free mass-spectrometry analysis (DIOS analysis) [91]. The main advantages associated are a simple realization of hydrophilic and functionalized pads in the superhydrophobic surface, allowing analytes trapping with an enhancement of the liquid/surface interaction, and a subsequent analysis by matrix-free desorption/ionization MS-DIOS on these pads.

Integration of the superhydrophobic electrodes inside a microfluidic microsystem, allowing low voltage actuation of a biological analyte and DIOS analysis is currently under investigation in our laboratory. Furthermore, the utilization of textured surfaces could prevent from non-specific sticking of bio particles, leading to an easy and efficient removal operation as compared to planar surface. Application such as particle sampling, concentration and analysis on superhydrophobic surfaces should be dedicated to environment control.

Conclusion

Among all the superhydrophobic surfaces displaying high roughness combined with low surface energy coating, trapping of air between the substrate and the liquid droplets is necessary to obtain a rolling ball effect (i.e. a quasi null hysteresis). Associated to an effective way to switch the wettability properties of the surface, control of droplet displacement on superhydrophobic surface seems to be possible. Unfortunately, only few techniques based on optical, electrical, mechanical or magnetic phenomenon, lead to a reversible modification of surface wettability. Among these techniques, electrowetting on classical surfaces (i.e. hydrophobic) seems to be the more mature technology. This is particularly emphasized by recent results on EWOD droplet liquid pixel and by the very last improvement concerning optical lenses integrated inside commercialized cellular phones (varioptic.com). Combining the amazing properties of superhydrophobic surfaces with reliable EWOD devices will open new opportunities for designing systems with potential applications based on specific properties of theses surfaces, in particular in the field of lab-on-chip (preparation of highly functional microfluidic devices), optical devices and controlled self cleaning surfaces. Concerning lab-on-chip devices, the most important effect expected, due to the quasi null hysteresis of these surfaces, is the liquid manipulation at very low tension voltage.

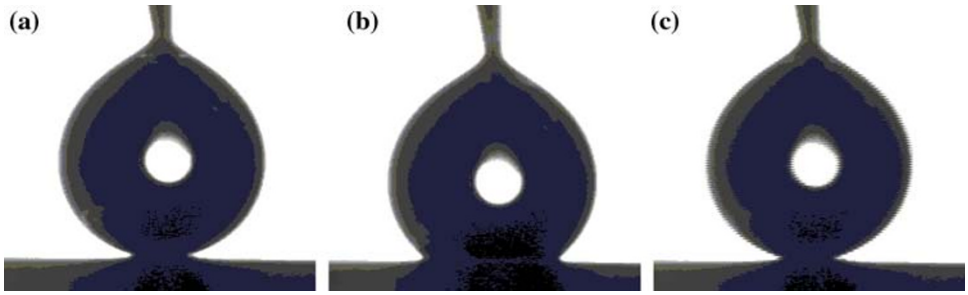

Fig. 31 Reversible EWOD observed on a drop deposited on a superhydrophobic silicon nanowires surface. (**a**) No tension applied, (**b**) a 150 V_{rms} tension applied (f = 1 kHz), (**c**) the tension is cut, the drop returns to its initial state

References

1. L. Feng, S. Li, H. Li, J. Zhai, Y. Song, L. Jiang, D. Zhu, Angew. Chem. Int. Ed. **41**, 1221 (2002)
2. L. Feng, Y. Song, J. Zhai, B. Liu, J. Xu, L. Jiang, D. Zhu, Angew. Chem. Int. Ed. **42**, 800 (2003)
3. M. Cao, X. Song, J. Zhai, J. Wang, Y. Wang, J. Phys. Chem. B **110**, 13072 (2006)
4. Y.C. Hong, H.S. Uhm, Appl. Phys. Lett. **88**, 244101 (2006)
5. K. Tadanaga, N. Katata, T. Minami, J. Am. Ceram. Soc. **80**, 1040 (1997)
6. E. Balaur, J.M. Macak, H. Tsuchiya, P. Schmuki, J. Mater. Chem. **15**, 4488 (2005)
7. W. Chen, A.Y. Fadeev, M.C. Hsieh, D. Oner, J. Youngblood, T.J. McCarthy, Langmuir **15**, 3395 (1999)
8. S.R. Coulson, I. Woodward, J.P.S. Badyal, S.A. Brewer, C.J. Willis, J. Phys. Chem. B **104**, 8836 (2000)
9. R. Fürstner, W. Barthlott, Langmuir **21**, 956 (2005)
10. J.-Y. Shiu, C.W. Kuo, P. Chen, C.Y. Mou, Chem. Mater. **16**, 561 (2004)
11. T.J. McCarthy, D. Oner, Langmuir **16**, 7777 (2000)
12. T. Young, Philos. Trans. R. Soc. Lond. **95**, 65 (1805)
13. J. Fox, W. Zisman, J. Colloid Interface Sci. **5**, 514 (1950)
14. W. Zisman, Chem. Ser. **43**, 381 (1964)
15. P-G de Gennes, F. Brochard-Wyart, D. Quere. Gouttes, bulles, perles et ondes. (Belin, collection Echelles, Paris, 2002)
16. http://www.bath.ac.uk/ceos/insects3.html
17. R.N. Wenzel, Ind. Eng. Chem. **28**, 988 (1936)
18. R.N. Wenzel, J. Phys. Colloid Chem. **53**, 1466 (1949)
19. A.B.D. Cassie, S. Baxter, Trans. Faraday Soc. **40**, 546 (1944)
20. R.E. Johnson, R.H. Dettre, Adv. Chem. Ser. **43**, 112 (1964)
21. J. Bico, Thèse, Université Paris VI (2000)
22. M. Nosonovsky, Langmuir **23**, 3157 (2007)
23. C. Yang, U. Tartaglino, B.N.J. Persson, Phys. Rev. Lett. **97**, 116103 (2006)
24. M. Callies, D. Quéré, Soft Matter **1**, 55 (2005)
25. D. Quéré, Physique statistique, Images de la Physique, CNRS 239 (2005)
26. J. Bico, U. Thiele, D. Quéré, Colloids Surf. A **206**, 41 (2002)
27. S. Shibuichi, T. Onda, N. Satoh, K. Tsujii, J. Phys. Chem. **100**, 19512 (1996)
28. J. Bico, C. Marzolin, D. Quéré, Europhys. Lett. **47**, 220 (1999)
29. Z. Yoshimitzu, A. Nakajima, T. Watanabe, K. Hashimoto, Langmuir **18**, 5818 (2002)
30. A. Lafuma, D. Quéré, Nature Mater. **2**, 457 (2003)
31. D. Quéré, A. Lafuma, J. Bico, Nanotechnology **14**, 1109 (2003)
32. S. Herminghaus, Europhys. Lett. **52**, 165 (2000)
33. N.A. Patankar, Langmuir **20**, 8213 (2004)
34. L. Gao, T.J. McCarthy, Langmuir. **22**, 2966 (2006)
35. K.K.S. Lau, J. Bico, K.B.K. Teo, M. Chlowalla, G.A.J. Amaratunga, W.I. Milne, G.H. McKinley, K.K. Gleason, Nano Lett. **3**, 1701 (2003)
36. L. Feng, S. Li, Y. Li, H. Li, L. Zang, J. Zhai, Y. Song, B. Liu, L. Jiang, D. Zhu, Adv. Mater. **14**, 1857 (2002)
37. H. Liu, J. Zhai, L. Jiang, Soft Matter. **2**, 811 (2006)
38. J. Lee, B. He, N. Patankar, J. Micromech. Microeng. **15**, 591 (2005)
39. T.H. Chen, Y.J. Chuang, C.C. Chieng, F.G. Tseng, J. Micromech. Microeng. **17**, 489 (2007)
40. J. Zhang, X. Lu, W. Huang, Y. Han, Macromol. Rapid Commun. **26**, 477 (2005)
41. M. Jin, X. Feng, L. Feng, T. Sun, J. Zhai, T. Li, L. Jiang, Adv. Mater. **17**, 1977 (2005)
42. X. Hong, X. Gao, L. Jiang, J. Am. Chem. Soc. **129**, 1478 (2007)
43. F. Zhou, W.T.S. Huck, Chem. Commun. 5999 (2005)
44. T.L. Sun, G.J. Wang, L. Feng et al., Angew. Chem. Int. Ed. **43**, 357 (2004)
45. Q. Fu, G.V.R. Rao, S.B. Basame, D.J. Keller, K. Artyushkova, J.E. Fulghum, G.P. Lopez, J. Am. Chem. Soc. **126**, 8904 (2004)
46. F. Xia, L. Feng, S. Wang, T. Sun, W. Song, W. Jiang, L. Jiang, Adv. Matter. **18**, 432 (2006)
47. A. Athanassiou, M.I. Lygeraki, D. Pisignano, K. Lakiotaki, M. Varda, E. Mele, C. Fotakis, R. Cingolani, S.H. Anastasiadis, Langmuir **22**, 2329 (2006)
48. H.S. Lim, J.T. Han, D. Kwak, M. Jin, K. Cho, J. Am. Chem. Soc. **128**, 14458 (2006)
49. W. Zhu, X. Feng, L. Feng, L. Jiang, Chem. Commun. 2753 (2007)
50. X. Feng, L. Feng, M. Jin, J. Zhai, L. Jiang, D. Zhu, J. Am. Chem. Soc. **126**, 62 (2004)
51. C. Takei, M. Nonogi, A. Hibara, T. Kitamori, H.B. Kim, Lab on Chip **7**, 596 (2007)
52. E. Balaur, J.M. Macak, L. Taveira, P. Schmuki, Electrochem. Commun. **7**, 1066 (2005)
53. Y. Coffinier, S. Janel, A. Addad, R. Blossey, L. Gengembre, E. Payen, R. Boukherroub, Langmuir **23**, 1608 (2007)
54. G. Lippmann, Ann. Chim. Phys. **5**, 494 (1875)
55. B. Berge, C. R. Acad. Sci. Paris série II **317**, 157 (1993)
56. Y. Fouillet, D. Jary, A.G. Brachet, J. Berthier, R. Blervaque, L. Davoux, J.M. Roux, J.L. Achard, C. Peponnet, 4th International Conference on Nanochannels, Microchannels and Minichannels, Liemrick, Ireland, June 19–21 (2006)
57. A. Froumkine, Actualités Sci. Ind. **373**, 1 (1936)
58. T.B. Jones, Langmuir **18**, 4437 (2002)
59. K.H. Kang, Langmuir **18**, 10318 (2002)
60. J. Buehrle, S. Herminghaus, F. Mugele, Phys. Rev. Lett. **91**, 086101 (2003)
61. M. Bienia, M. Vallade, C. Quilliet, F. Mugele, Europhys. Lett. **74**, 103 (2006)
62. F. Mugele, J. Buerhle, J. Phys.: Condens. Matter **19**, 375112 (2007)
63. S. Kuiper, 5th International Meeting on Electrowetting, Rochester (NY, USA), May 31–June 2 (2006)
64. A. Torkelli, Droplet microfluidics on planar surface, ISBN 951-38-6237-2 (2003)
65. H.J.J. Verheijen, M.W.J. Prins, Langmuir **15**, 6616 (1999)
66. M. Vallet, M. Vallade, B. Berge, Eur. Phys. J. B **11**, 583 (1999)
67. B. Shapiro, H. Moon, R.L. Garrell, C.J. Kim, J. Appl. Phys. **93**, 5794 (2003)
68. F. Mugele, J.C. Baret, J. Phys.: Condens. Matter. **17**, R705 (2005)
69. R.D. Fair, Microfluid Nanofluid **3**, 245 (2007)
70. B. Berge, J. Peseux, Eur. Phys. J. E **3**, 159 (2000)
71. Varioptic, http://www.varioptic.com
72. H. Pellat, C. R. Acad. Sci. Paris. **119**, 691 (1895)
73. N.R. Smith, D.C. Abeysinghe, J.W. Haus, J. Heikenfeld, Optics Express. **14**, 6557 (2006)
74. Liquavista, http://www.liquavista.com
75. R.A. Hayes, B.J. Feenstra, Nature **425**, 383 (2003)
76. J. Heikenfeld, A.J. Steckl, Appl. Phys. Lett. **86**, 011105 (2005)
77. S.K. Cho, H. Moon, C.J. Kim, J. Microelec. Sys. **12**, 70 (2003)
78. J. Berthier, P. Silberzan, Microfluidics for Biotechnology (Artech House Publishers 2005)
79. M.G. Pollack, R.B. Fair, A.D. Shenderov, Appl. Phys. Lett. **77**, 1725 (2000)
80. M.G. Polack, A.D. Shenderov, R.B. Fair, Lab Chip **2**, 101 (2002)
81. V. Srinivasan, V.K. Pamula, R.B. Fair, Lab Chip. **4**, 310 (2004)
82. A.R. Wheeler, H. Moon, C.A. Bird, R.R. Ogorzalek Loo, C.J. Kim, J.A. Loo, R.L. Garrell, Anal. Chem. **77**, 534 (2005)
83. F. Caron, J.-C. Fourrier, C. Druon, P. Tabourier, French Patent N° FR 0406080 issued on 2005

84. Y. Fouillet, H. Jeanson, I. Chartier, A. Buguin, P. Silberzan, Houille blanche, Revue Internationale de l'Eau **4**, 37 (2003)
85. T.N. Krupenkin, J.A. Taylor, T.M. Schneider, S. Yang, Langmuir **20**, 3824 (2004)
86. T. Krupenkin, J.A. Taylor, P. Kolodner, M. Hodes, Bell Labs Tech. J. **10**, 161 (2005)
87. D.L. Herbertson, C.R. Evans, N.J. Shirtcliffe, G. McHale, M.I. Newton, Sens. Actuators A **130**, 189 (2006)
88. M.S. Dhindsa, N.R. Smith, J. Heikenfeld, P.D. Rack, J.D. Fowlkes, M.J. Doktycz, A.V. Melechko, M.L. Simpson, Langmuir **22**, 9030 (2006)
89. A. Klingner, F. Mugele, J. Appl. Phys. **95**, 2918 (2004)
90. K. Bhat, J. Heikenfeld, M. Agarwal, Y. Lvov, K. Varahramyan, Appl. Phys. Lett. **91**, 024103 (2007)
91. N. Verplanck, Y. Coffinier, M. Wisztorski, G. Piret, C. Delhaye, V. Thomy, I. Fournier, J.-C. Camart., P. Tabourier, R. Boukherroub, The 10th International Conference on Miniaturized Systems for Chemistry and Life Sciences (μTAS Tokyo) 771 (2006)
92. N. Verplanck, Y. Coffinier, E. Galopin, J.-C. Camart, V. Thomy, R. Boukherroub, Nano Lett. **3**, 813 (2007)